

Series Editor
Robert Baptist

Nonlinear Electronics 2

Flip-Flops, ADC, DAC and PLL

Brahim Haraoubia

Color section

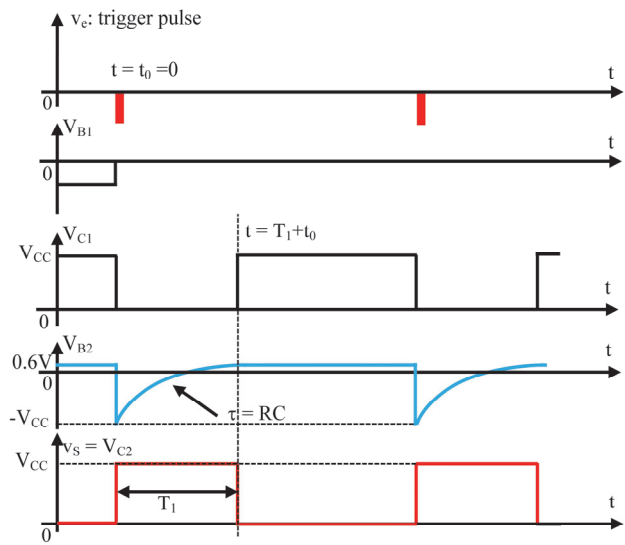


Figure 1.6. Signals associated with the functioning of the bipolar transistor monostable

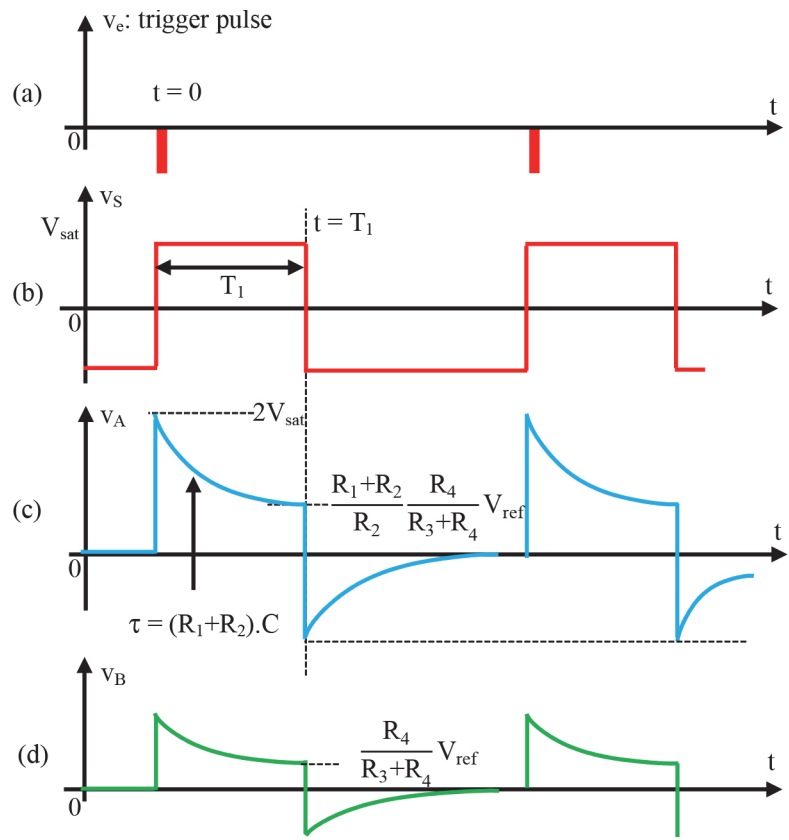


Figure 1.9. Evolution of the different signals at the level of the op-amp monostable: (a) triggering signal; (b) output signal; (c) signal at point A; (d) signal at point B

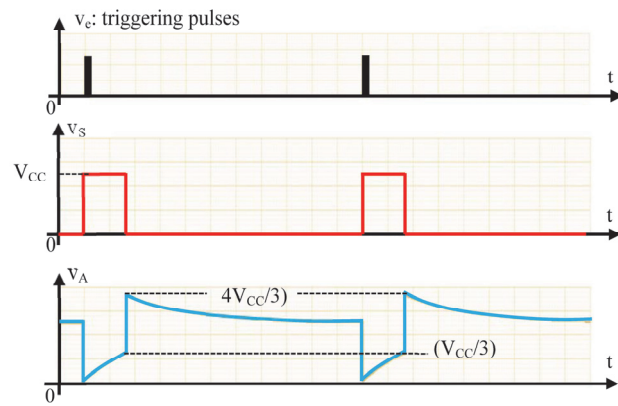


Figure 1.13. Signals implemented in a NOR gate monostable

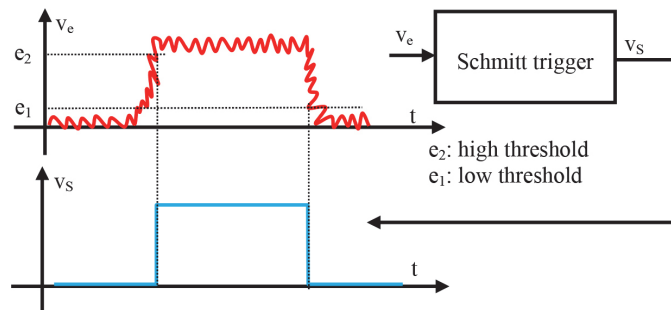


Figure 1.26. Application example of the Schmitt trigger: reshaping of a square wave

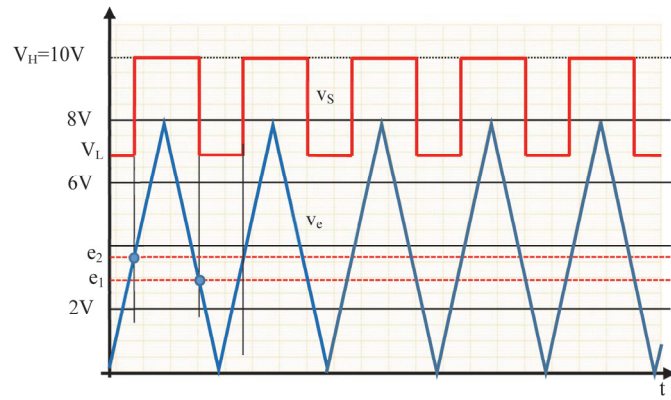


Figure 1.31. Variation of the output signal corresponding with the signal applied to the input of the bipolar transistor Schmitt trigger

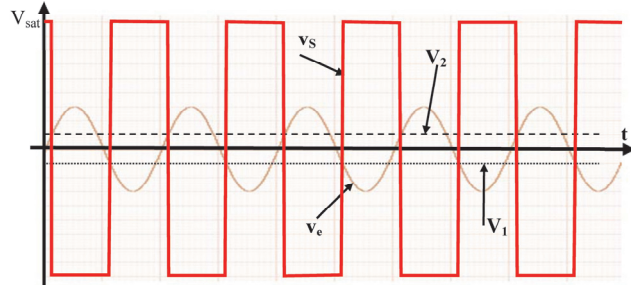


Figure 1.33. Evolution of the output signal v_s compared to the signal v_e applied to the input of an op-amp Schmitt trigger

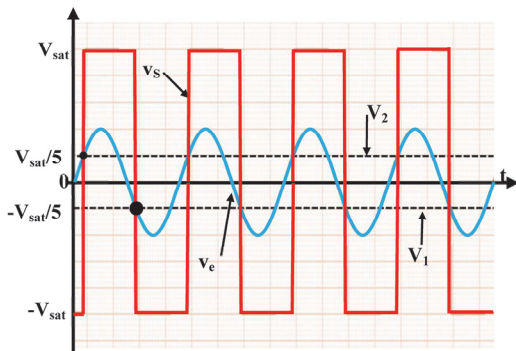


Figure 1.36. Signals involved at the non-inverting Schmitt trigger level

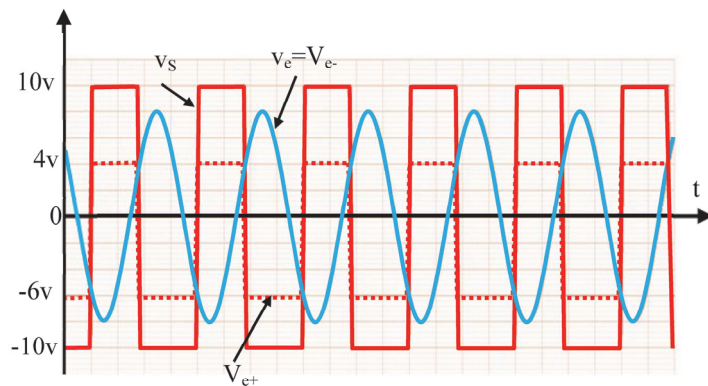


Figure 1.39. Signals involved in a Schmitt trigger with adjustable thresholds

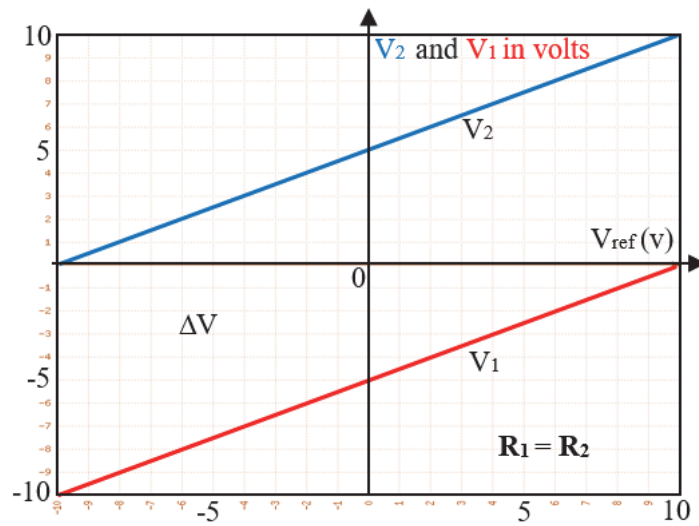


Figure 1.40. Evolution of switching thresholds based on the reference voltage V_{ref}

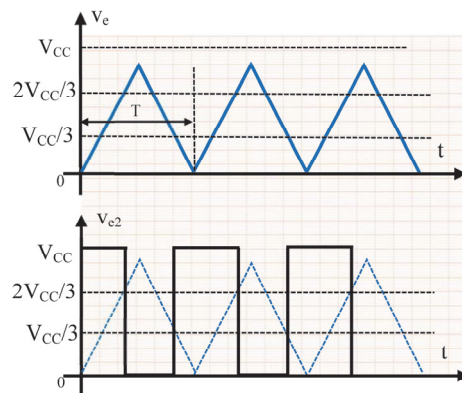


Figure 1.42. Evolution of the output signal according to the signal applied to the input of a Schmitt trigger designed around the 555 circuit

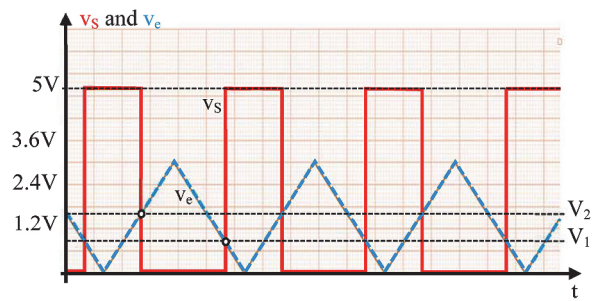


Figure 1.46. Evolution of the output signal according to the signal applied to the input Schmitt trigger based on the 7414 IC

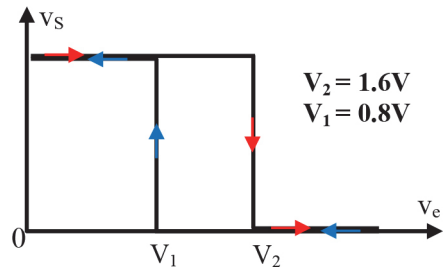


Figure 1.47. Hysteresis cycle of the Schmitt trigger based on the 7414 circuit

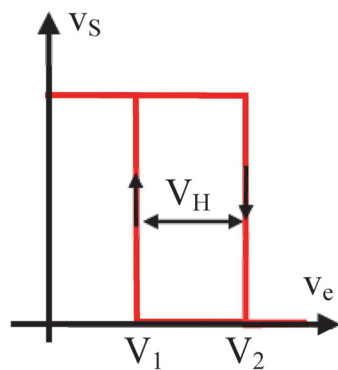


Figure 1.50. Hysteresis cycle of the built-in Schmitt trigger of the 4093 circuit

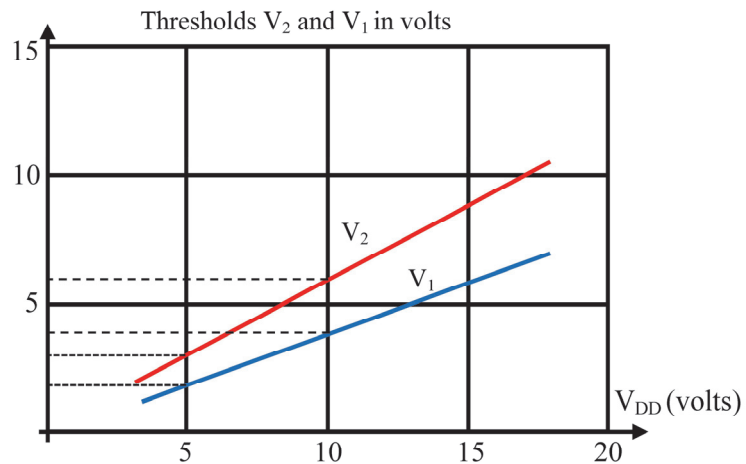


Figure 1.51. Evolution of the switching thresholds with the supply voltage
(source: datasheet Texas Instruments)

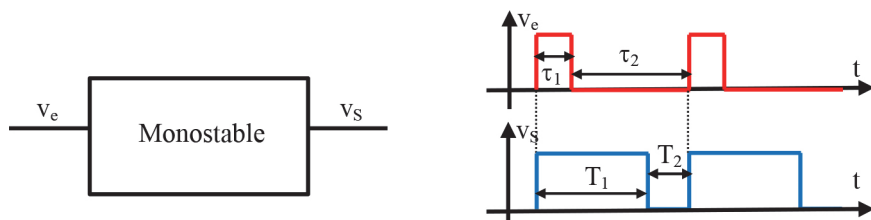


Figure E1.1. (a) Monostable circuit and (b) signals involved

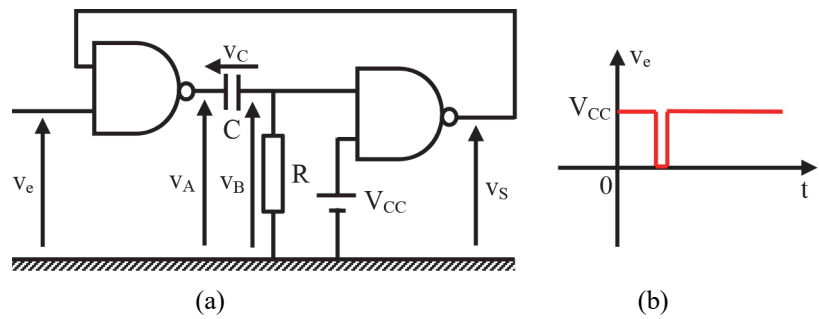


Figure E2.1. (a) Circuit under study and (b) pulse applied on input

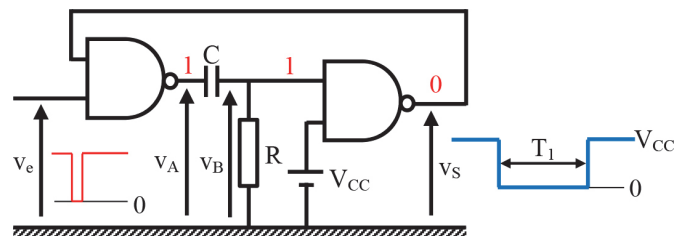


Figure E2.2. Quasi-stable state of the circuit

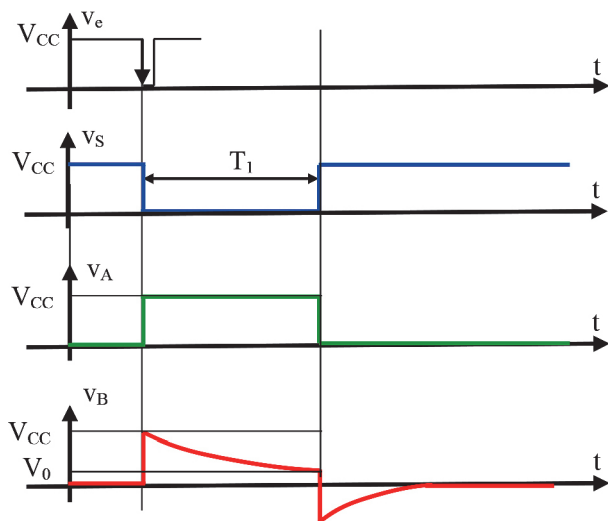


Figure E2.3. Representation over the time of voltages v_A , v_B and v_S

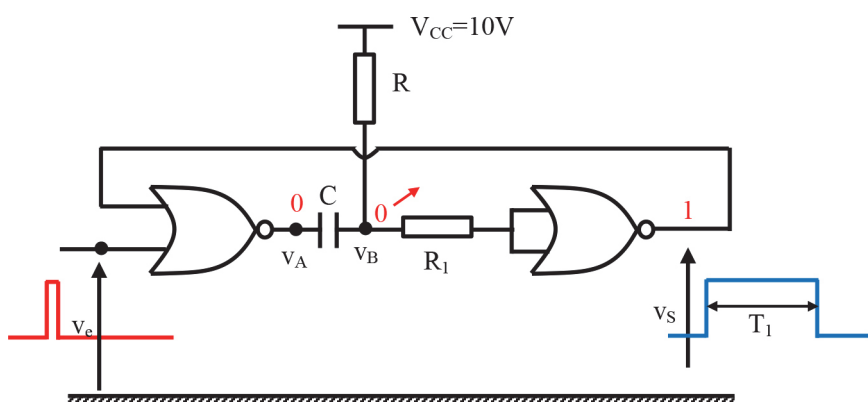


Figure E3.2. Switching of the stable state to the quasi-stable state

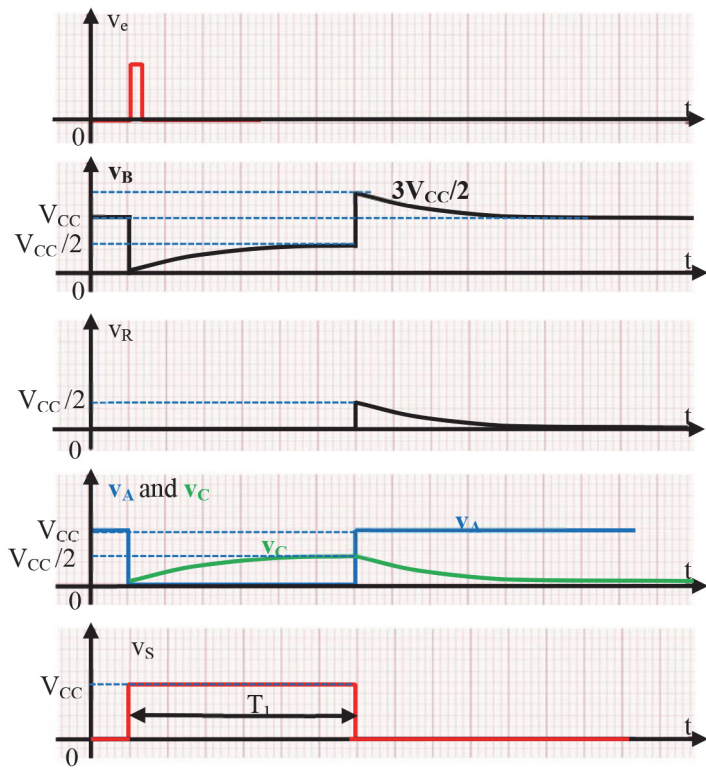


Figure E3.3. Representation of voltages v_A , v_B , v_R , v_C and v_s

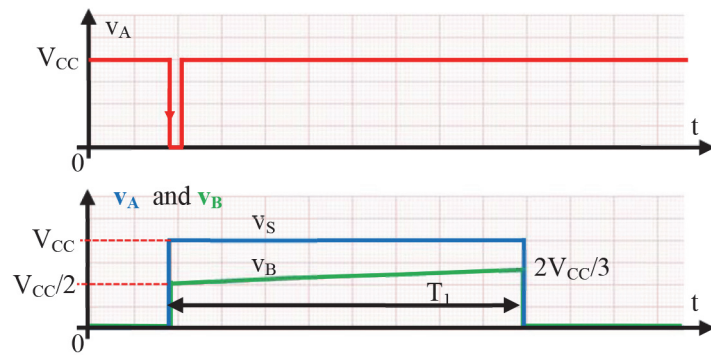


Figure E4.2. Evolution of voltages v_A , v_B and v_s

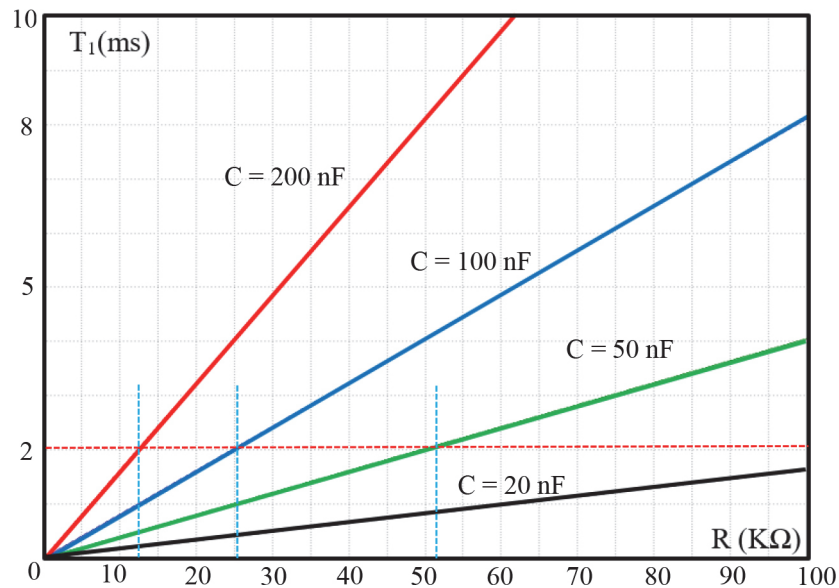


Figure E4.3. Evolution of the duration of the quasi-stable state according to R

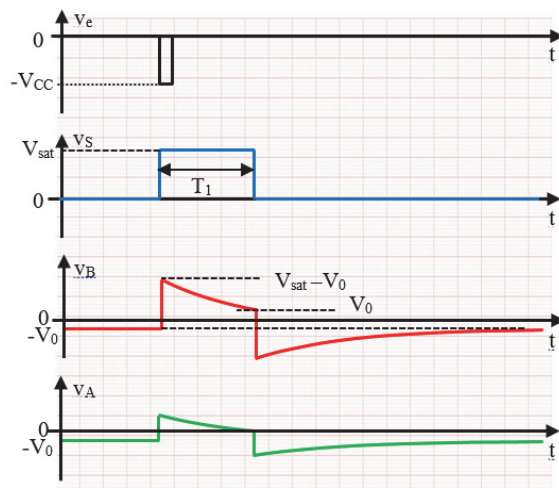


Figure E5.3. Evolution in time of the signals v_e , v_s , v_B and v_A

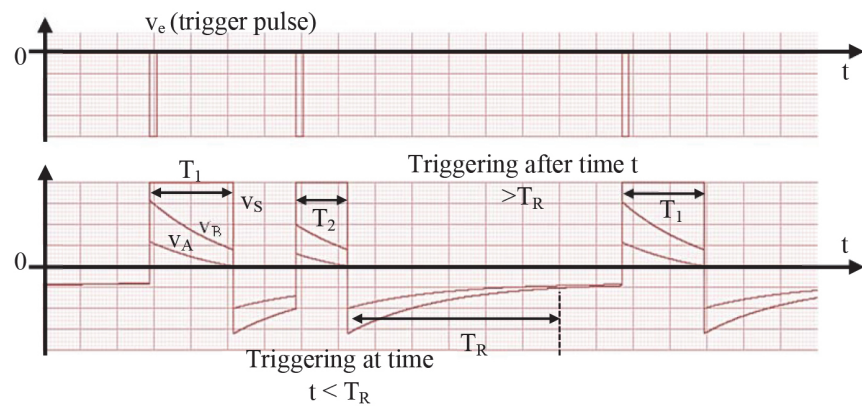


Figure E5.4. Effect of the recovery time on the monostable operation

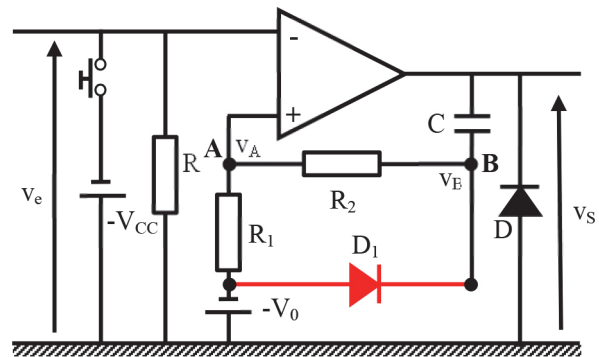


Figure E5.5. Insertion of diode D_1 to decrease the recovery time

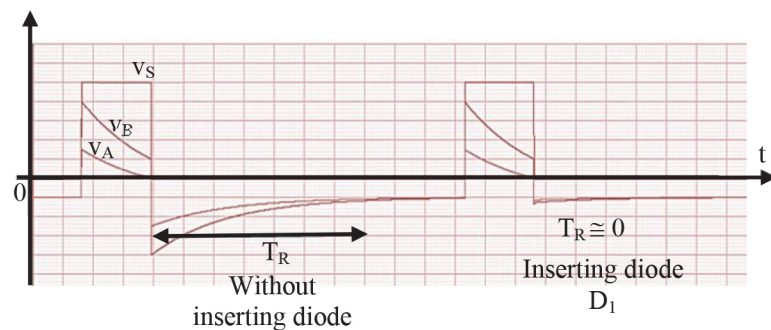


Figure E5.6. Effect of the diode on the recovery time

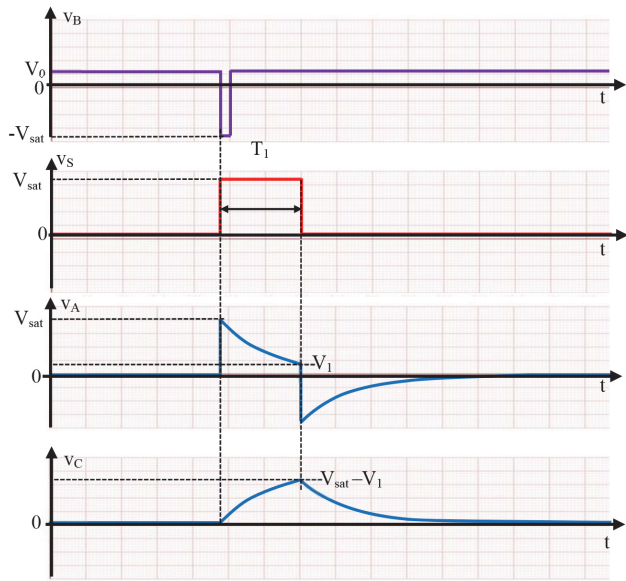


Figure E6.2. Representation of the evolution over time of the signals at points B, S, A and at the terminals of capacitor C for $V_1 > 0$

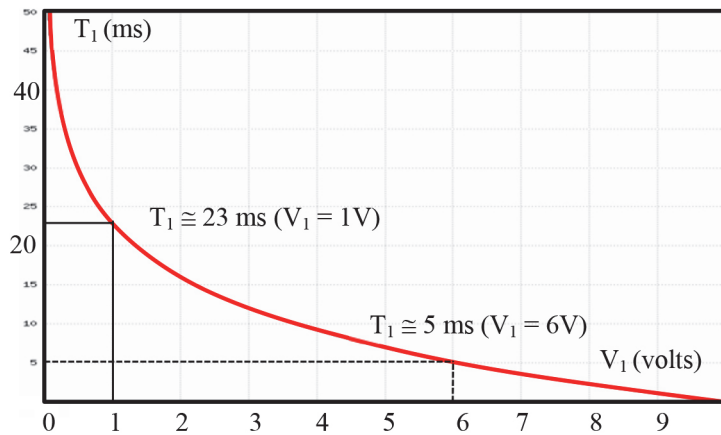


Figure E6.3. Evolution of the duration of the quasi-stable state according to voltage V_1

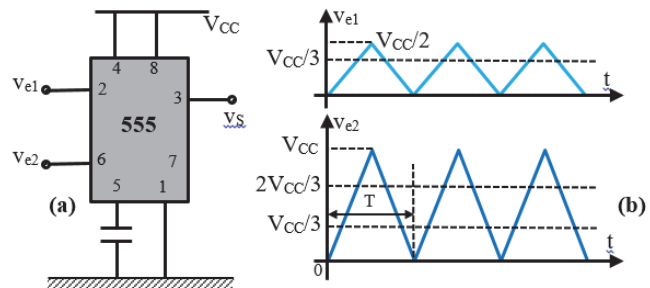


Figure E7.1. (a) Circuit under study and (b) signals applied on the inputs

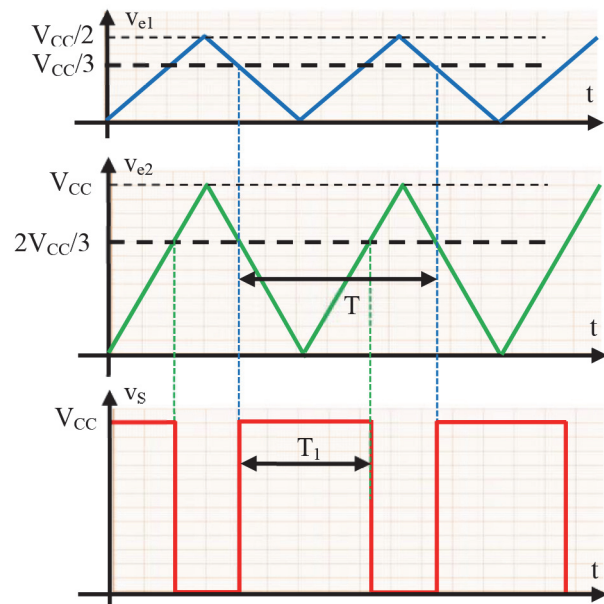


Figure E7.3. Representation of the evolution of the output voltage according to v_{e1} and v_{e2}

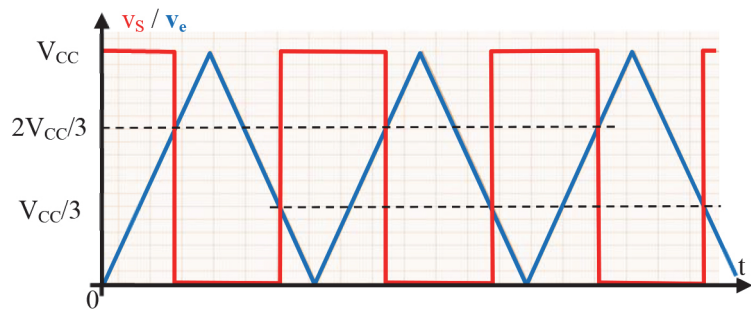


Figure E7.4. Evolution of the output voltage v_s according to time

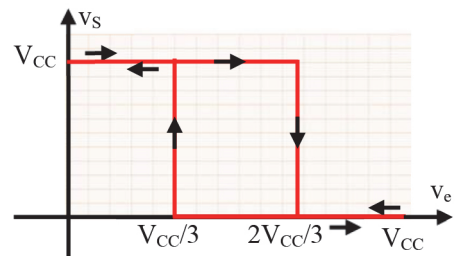


Figure E7.5. Evolution of the output voltage v_s according to time

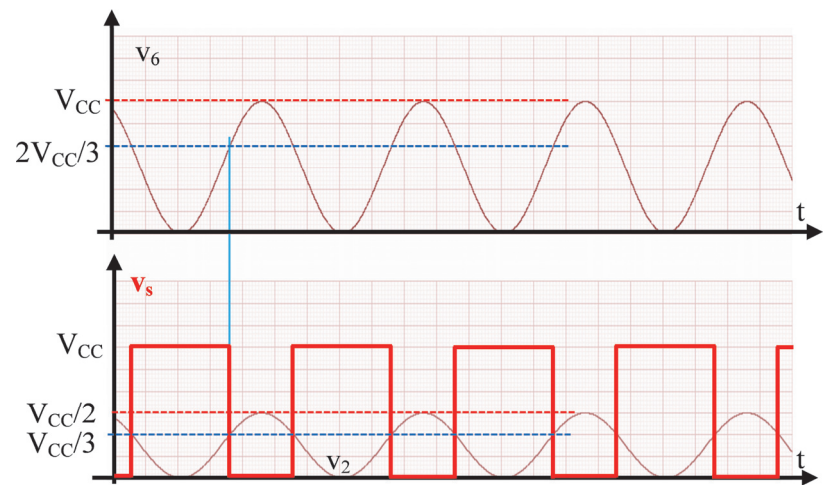


Figure E7.6. Evolution of the output voltage v_6 with respect to time

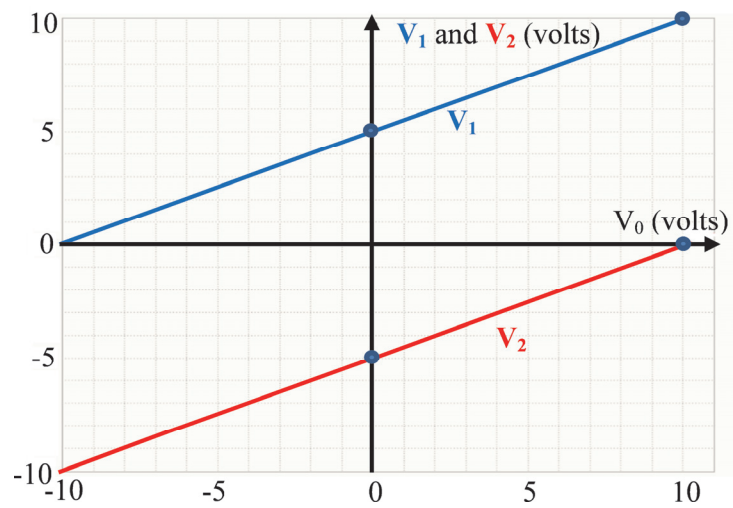


Figure E8.2. Evolution of the switching thresholds according to V_0

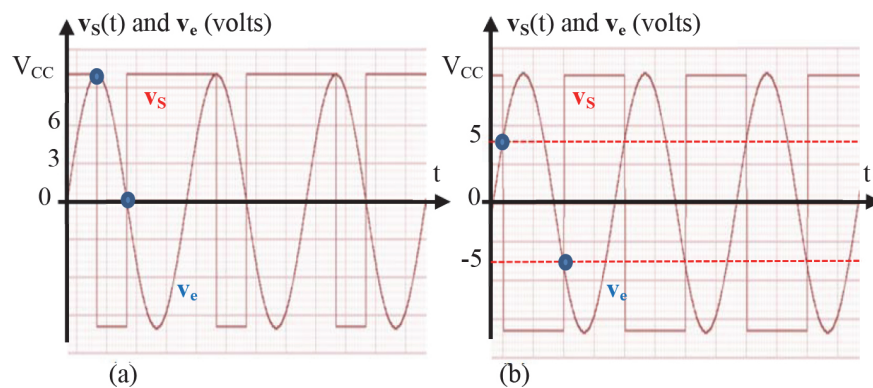


Figure E8.3. Representation of $v_s(t)$: (a) $V_0 = V_{cc}$ and (b) $V_0 = 0$

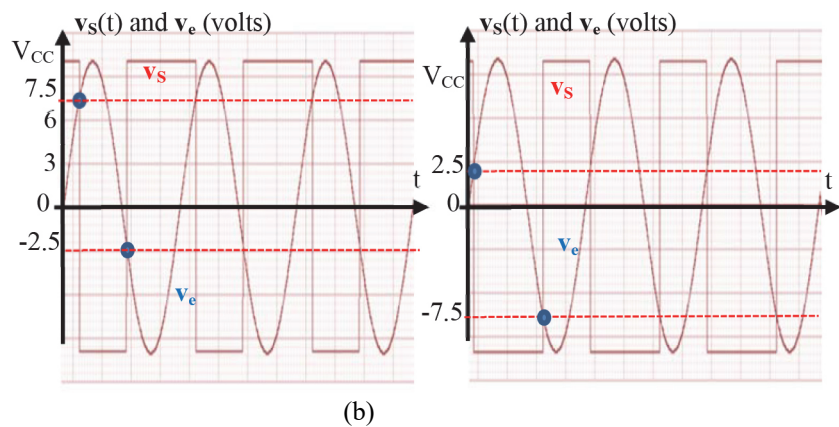


Figure E8.4. Representation of $v_s(t)$: (a) $V_0 = V_{cc}/2$ and (b) $V_0 = (-V_{cc}/2)$

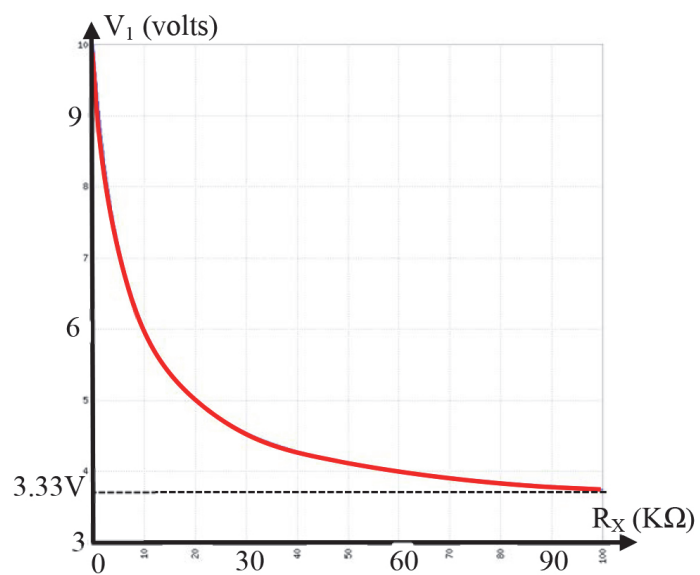


Figure E9.2. Evolution of the high switching threshold according to R_x

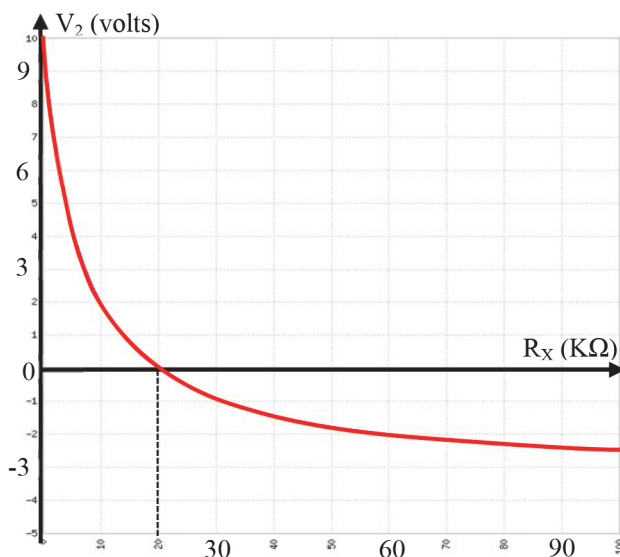


Figure E9.3. Evolution of the low switching threshold according to R_X

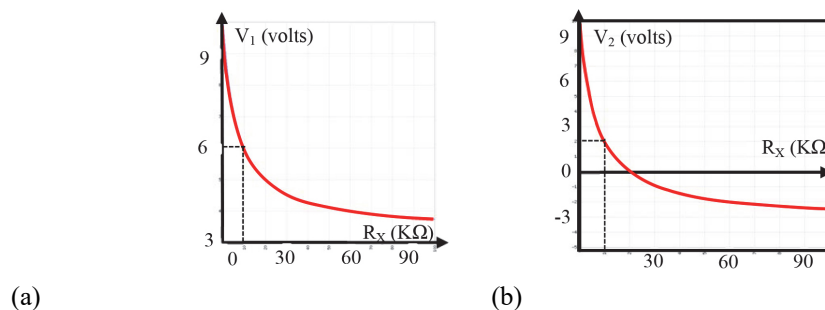


Figure E9.4. Graphical determination of the switching thresholds for $R_X = 10 k\Omega$: (a) high threshold and (b) low threshold

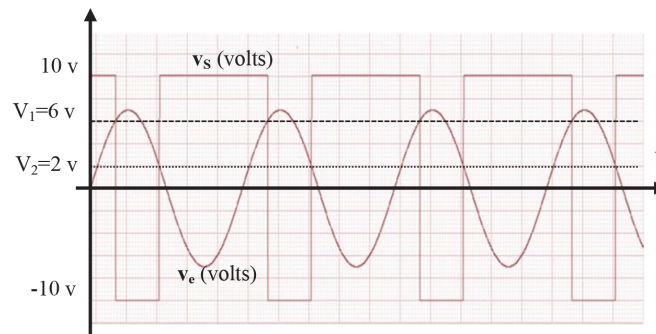


Figure E9.5. Evolution of the output voltage with respect to time according to the input voltage

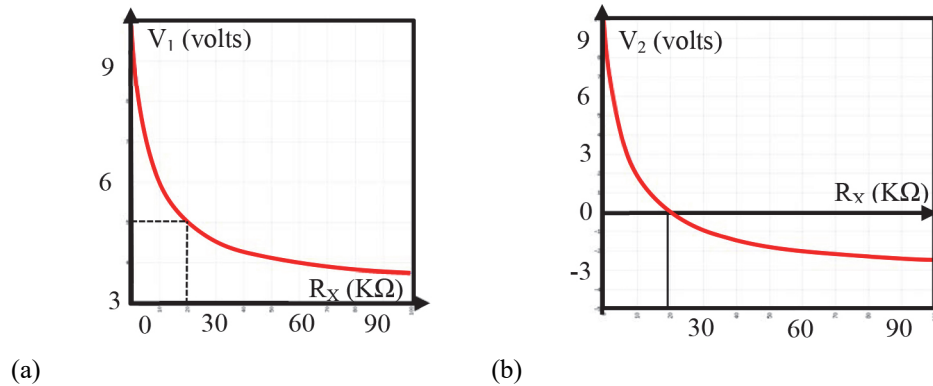


Figure E9.6. Graphical determination of switching thresholds for $R_X = 20 \text{ k}\Omega$:
(a) high threshold and (b) low threshold

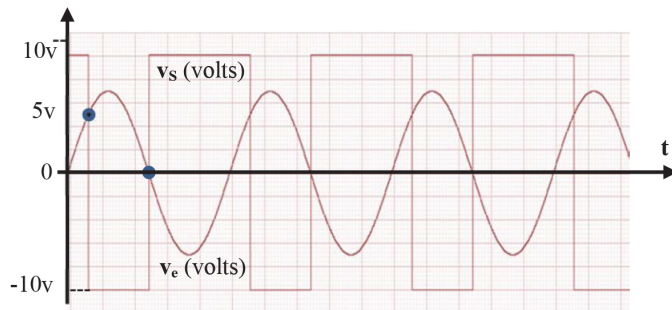


Figure E9.7. Evolution of the output voltage with respect to time

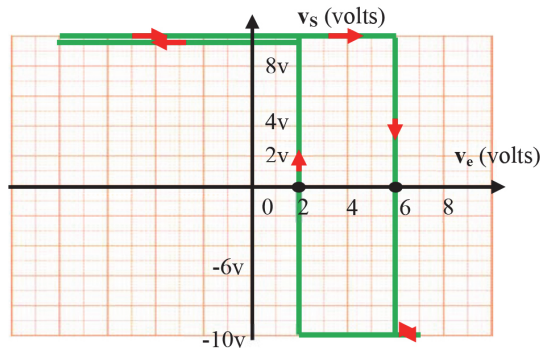


Figure E9.8. Evolution of $v_s = f(v_e)$ for $R_x = 10 \text{ k}\Omega$

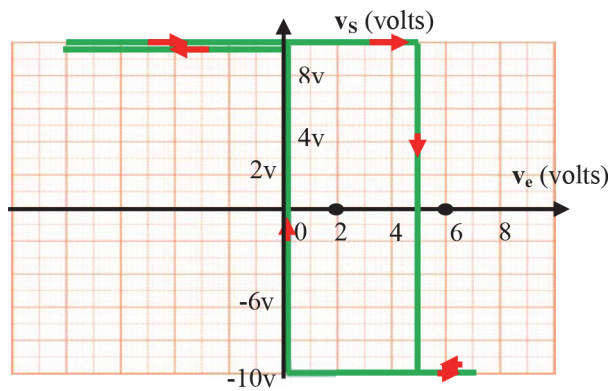


Figure E9.9. Evolution of $v_s = f(v_e)$ for $R_x = 20 \text{ k}\Omega$

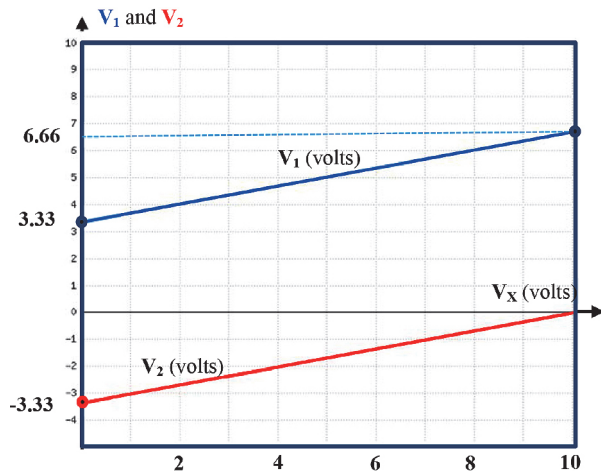


Figure E9.10. Evolution of the high threshold V_1 and the low threshold V_2 according to voltage V_x

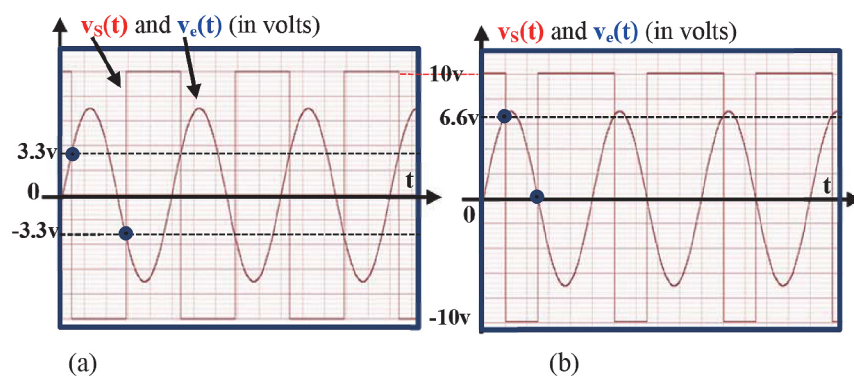


Figure E9.11. Plot of $v_s(t)$: (a) $V_x = 0 \text{ V}$ and (b) $V_x = V_{CC} = 10 \text{ V}$

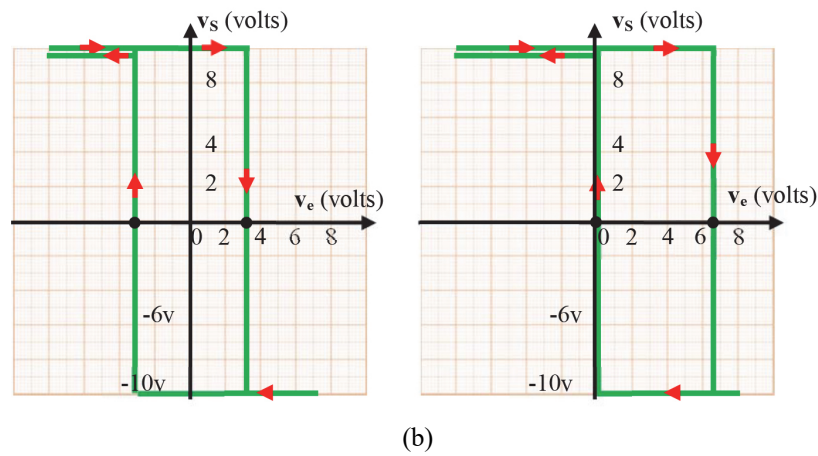


Figure E9.12. Plot of $vs = f(ve)$: (a) $VX = 0\text{ V}$ and (b) $VX = VCC = 10\text{ V}$

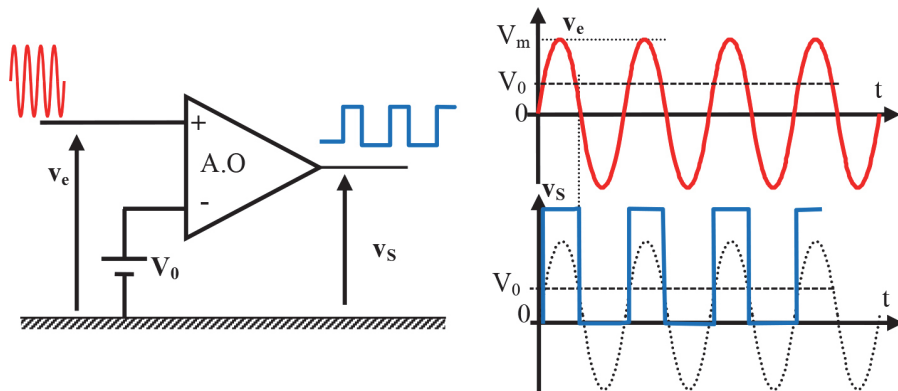


Figure 2.5. The output of the comparator gives at all times information about the amplitude of the input signal with respect to a reference voltage V_0

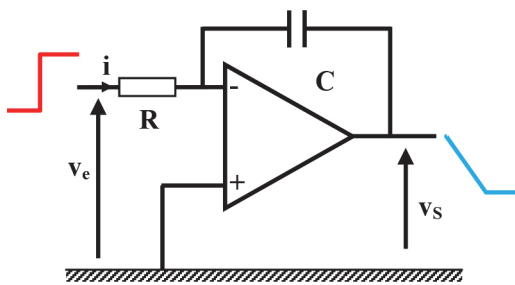


Figure 2.6. Op-amp integrator circuit

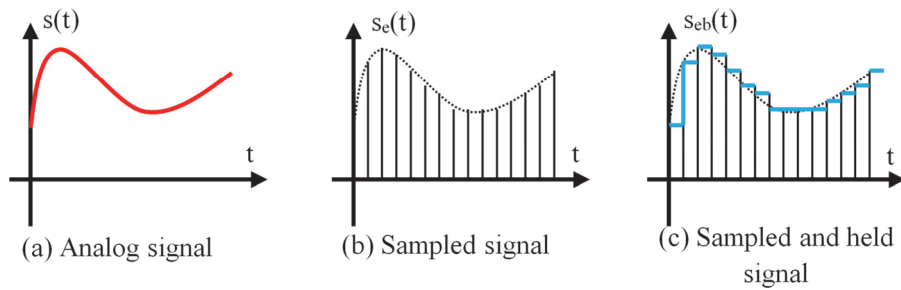


Figure 2.12. Sample-and-hold principle

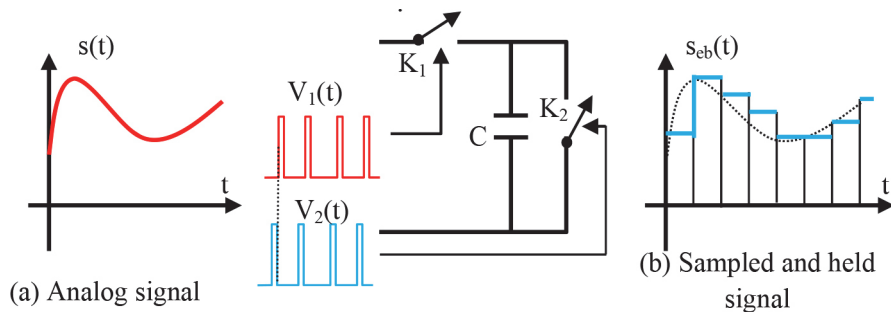


Figure 2.13. Basic sample-and-hold circuit

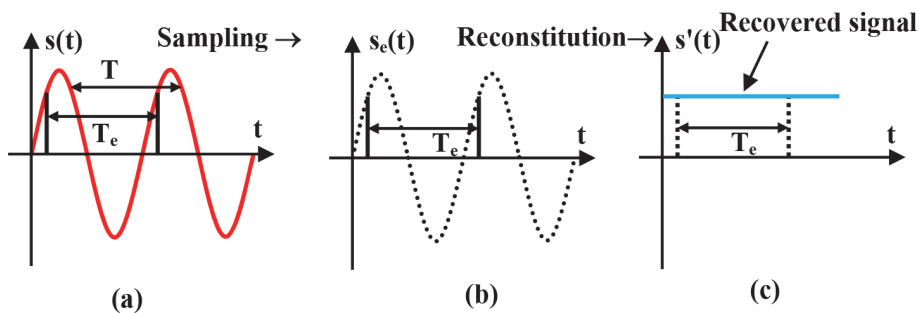


Figure 2.14. Sampling and reconstitution of the original signal when the sampling frequency is equal to the frequency of the original signal

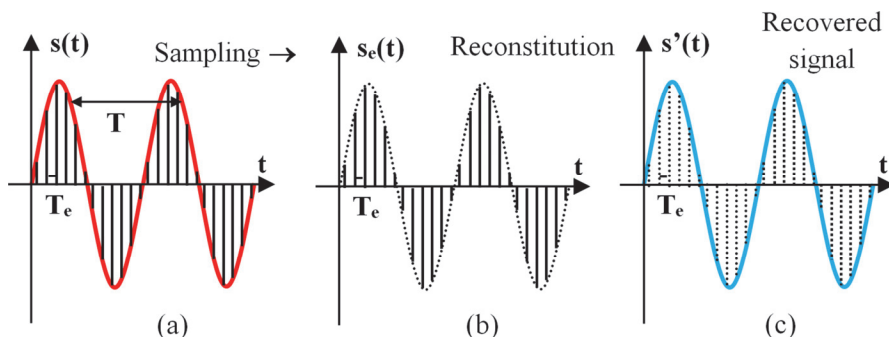


Figure 2.15. Sampling and reconstruction of the original signal when the sampling frequency is very large compared to the maximal frequency of the signal

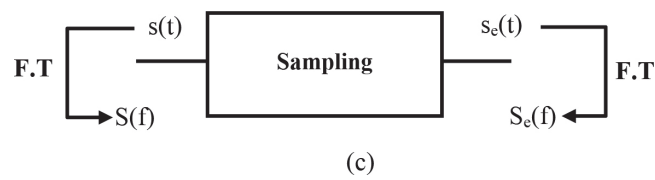
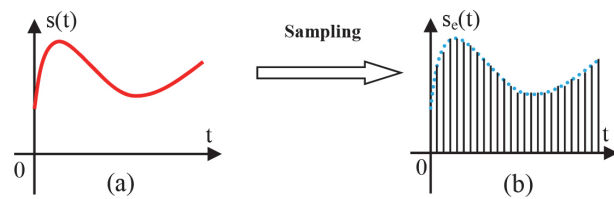


Figure 2.17. (a) Analog signal $s(t)$ to be processed. (b) Corresponding sampled signal. (c) Each signal has its own frequency spectrum

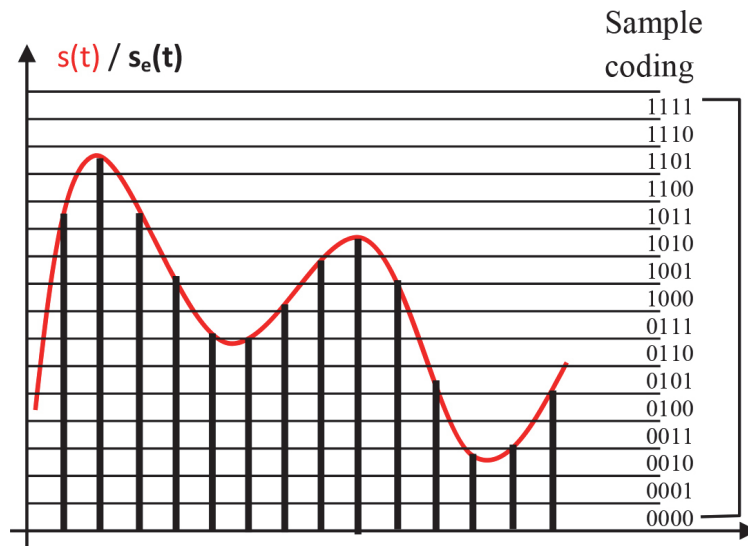


Figure 2.27. Quantification operation

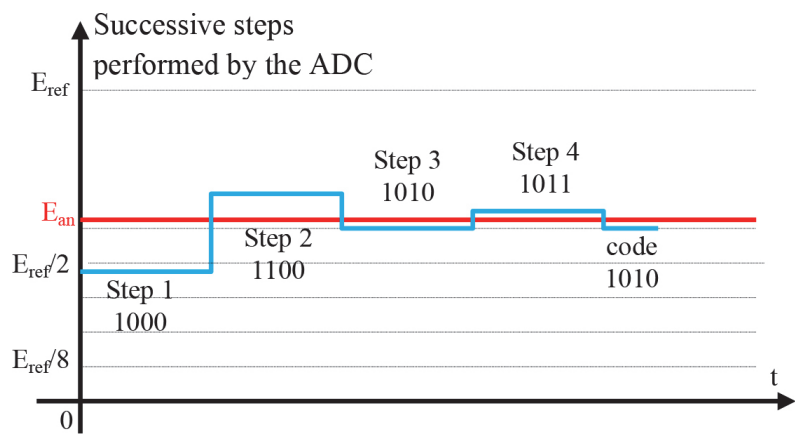


Figure 2.34. Various steps to obtain the code for an analog sample for a successive approximation ADC

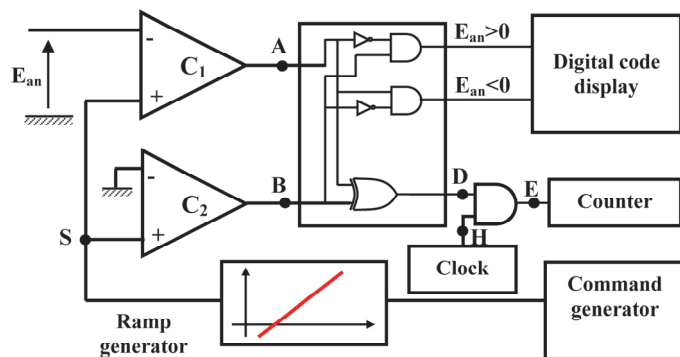


Figure 2.36. Schematic diagram of a single-ramp converter

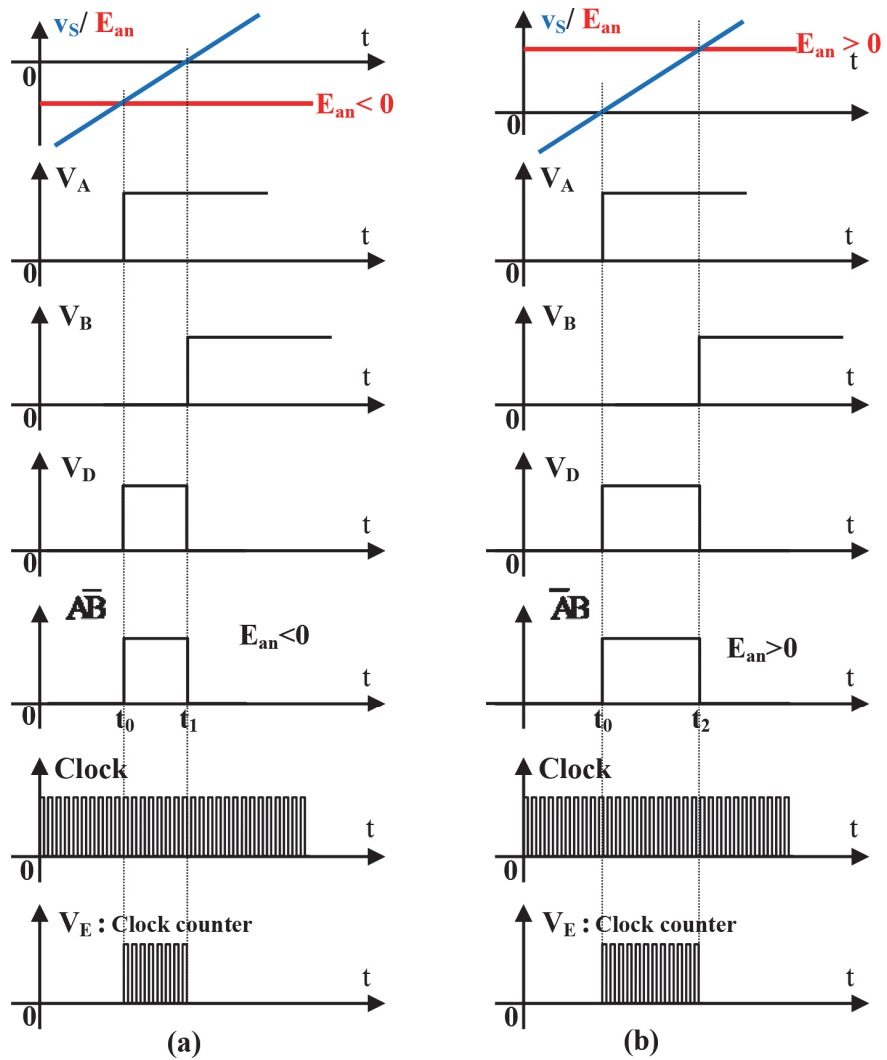


Figure 2.38. (a) Signals involved during conversion of a negative sample, (b) signals involved during conversion of a positive sample

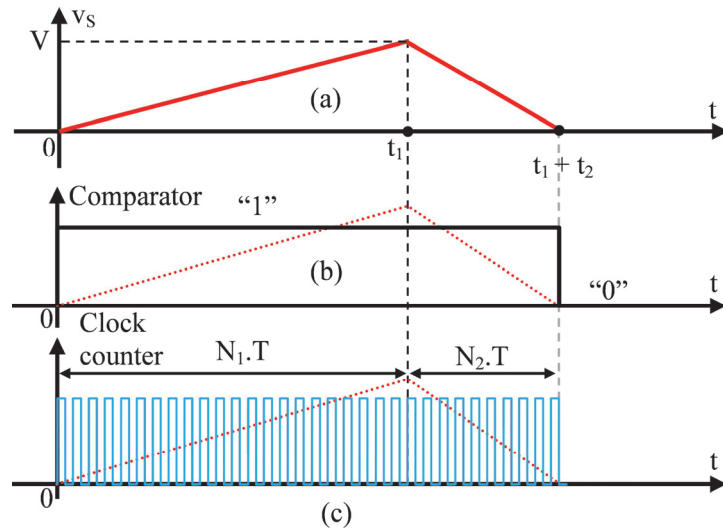


Figure 2.43. Different signals at the dual-slope ADC level

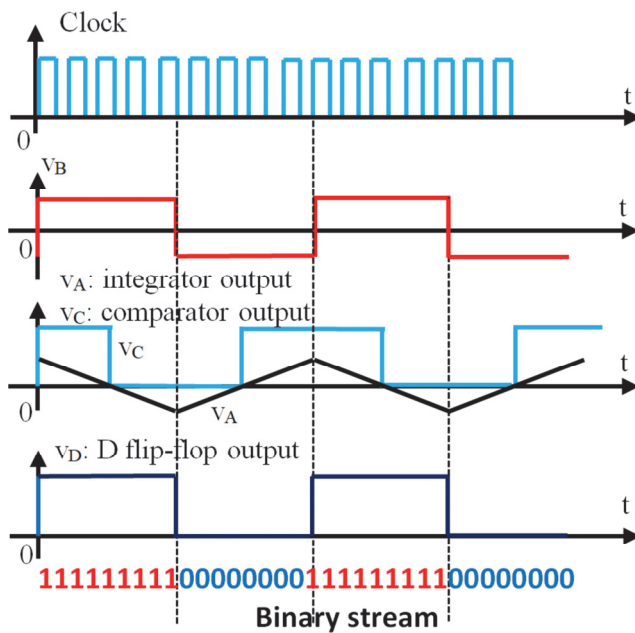


Figure 2.46. Signal representation at the level of the sigma-delta modulator with $E_{an} = 0$

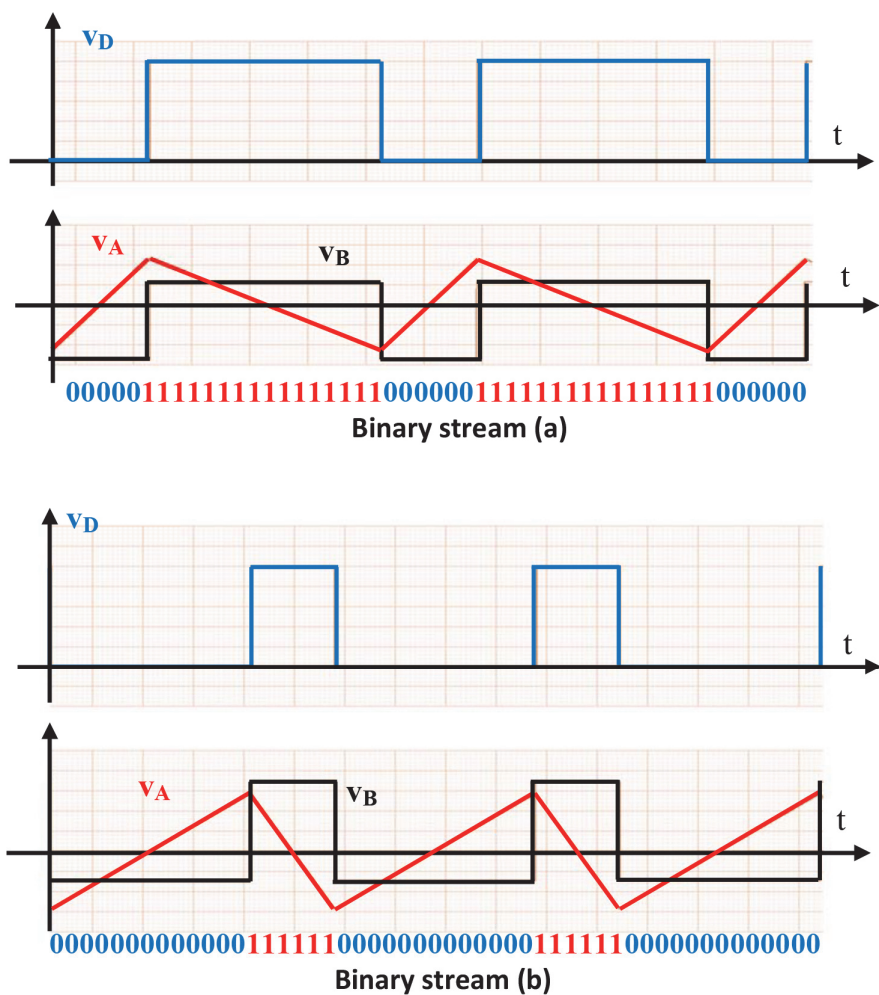


Figure 2.47. Signals identified in a sigma-delta ADC and binary output stream when (a) the sample $E_{an} > 0$ and (b) the sample $E_{an} < 0$

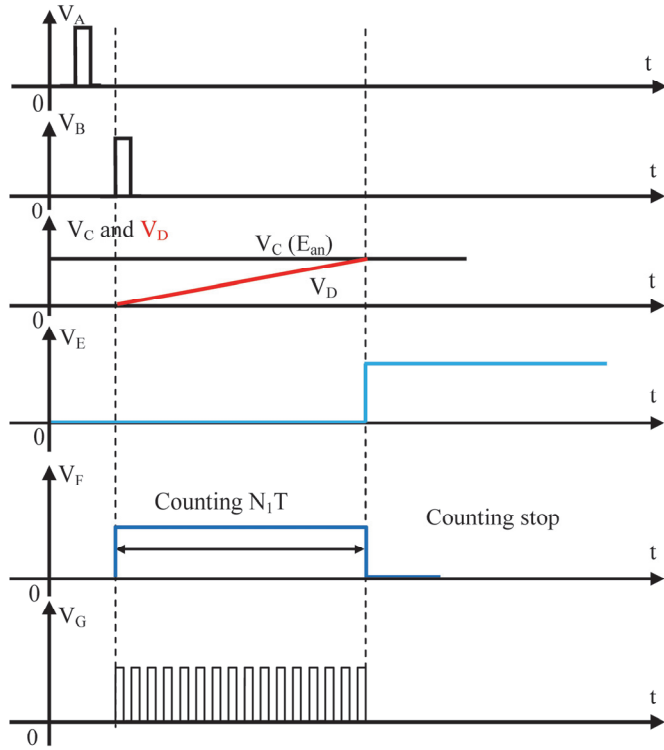


Figure E8.2. Signals involved at different points of the circuit presented in Figure E8.1

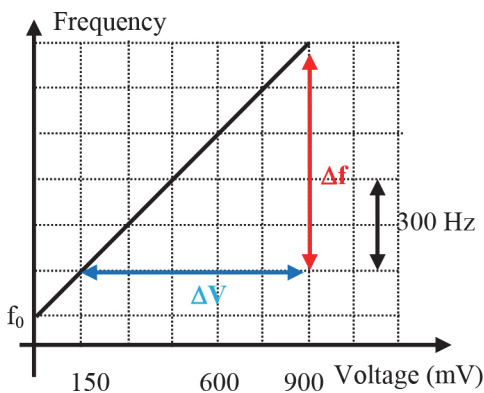


Figure E9.5. Slope of the VCO transfer curve

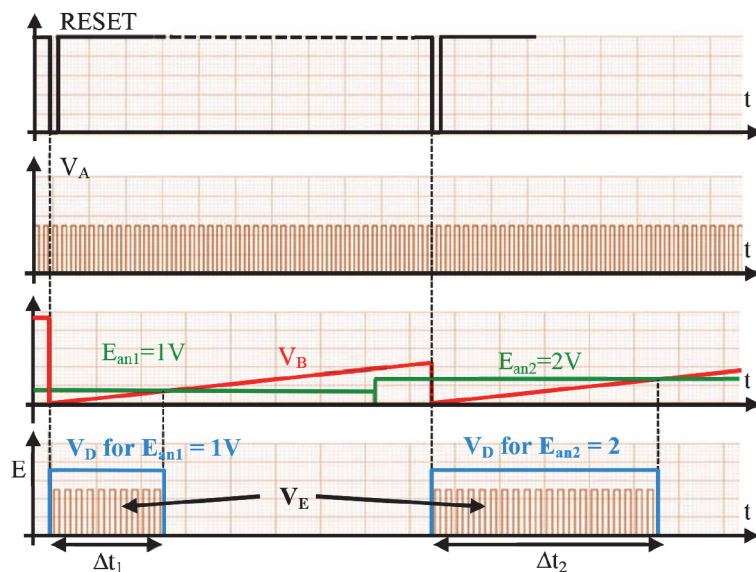


Figure E11.2. Evolution of various signals in the ADC under study

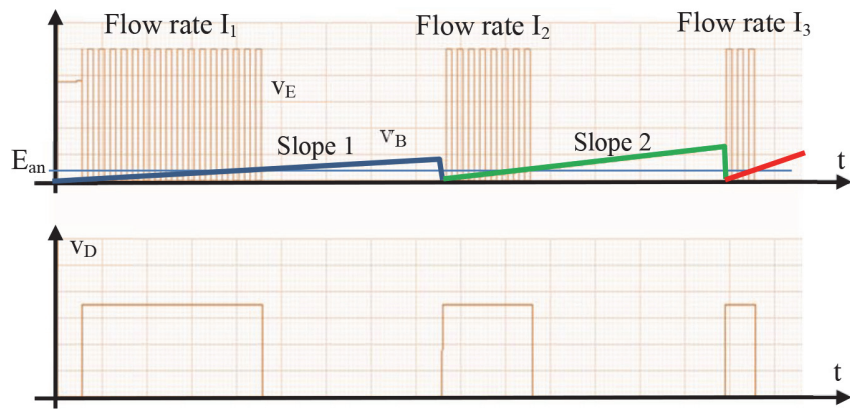


Figure E11.3. ADC accuracy in relation to the flow rate of the constant current generator with $I_1 < I_2 < I_3$

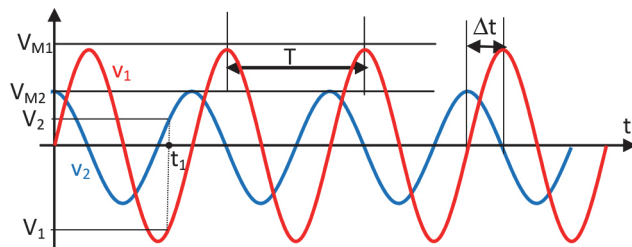


Figure 3.2. Phase shift between two signals

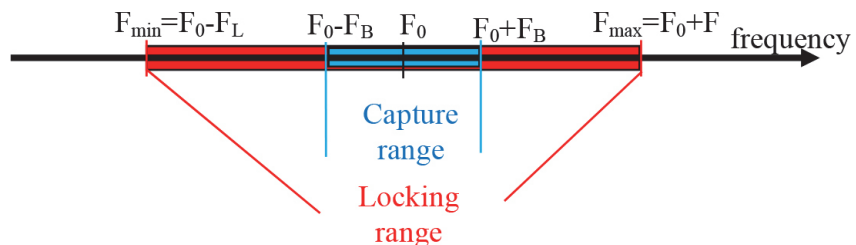


Figure 3.12. Capture range and locking range

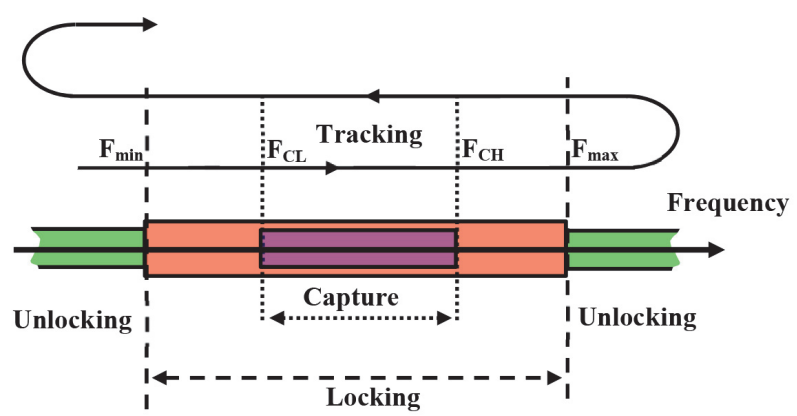


Figure 3.13. Operating mode of a PLL

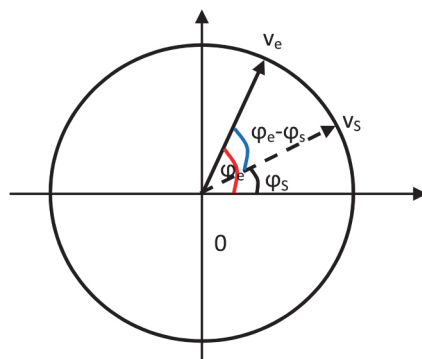


Figure 3.14. Vector representation of input and output signals

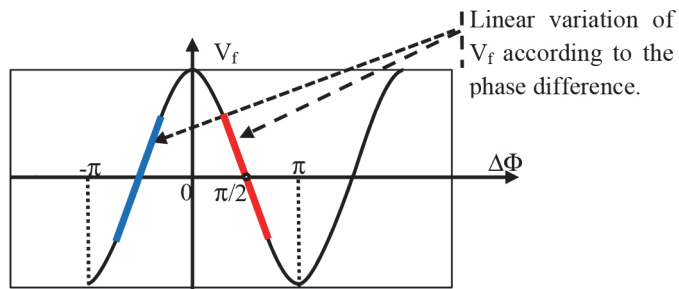


Figure 3.16. Evolution of the voltage V_f at the low-pass filter output based on the difference of phase shift $\Delta\Phi$. The variation is sinusoidal

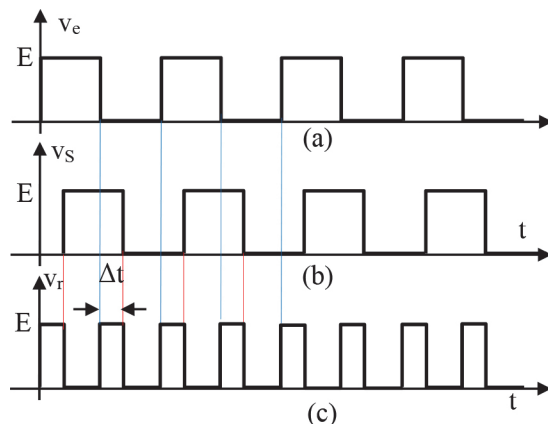


Figure 3.18. Various existing signals in a digital PLL. (a) reference signal v_e ; (b) signal v_s that can be found at the VCO output. (c) signal v_r that is found at the phase comparator output

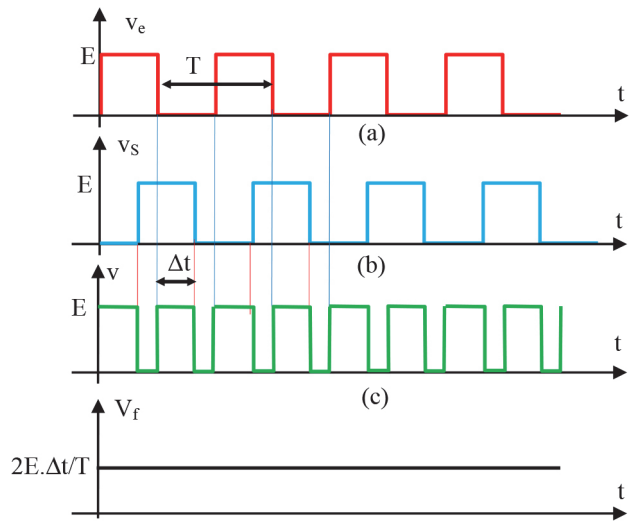


Figure 3.19. Different existing signals at the phase comparator input and output and the output of the low-pass filter ($0 < \Delta\phi < \pi$)

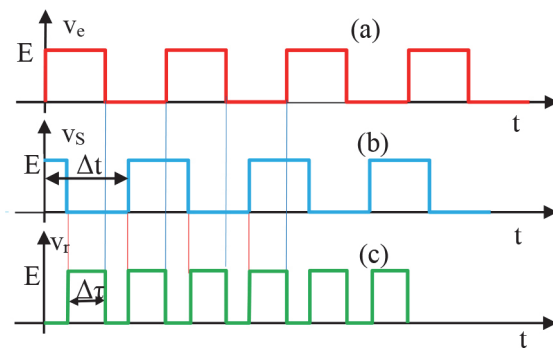


Figure 3.20. Signals at the phase comparator input and output when the phase shift is greater than π

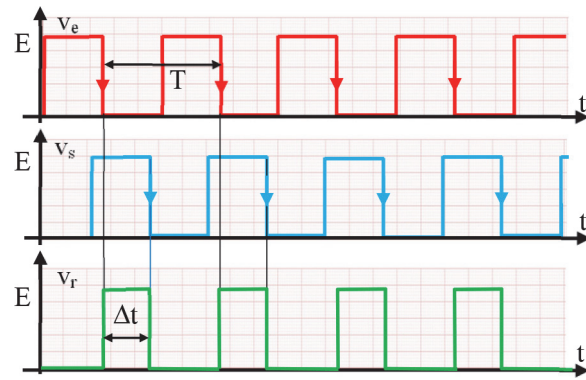


Figure 3.23. Evolution of signals at the RS flip-flop input and output of the phase comparator

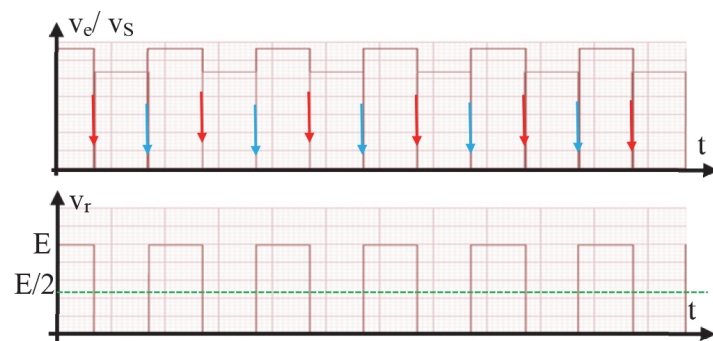


Figure 3.25. Phase comparator input and output signals

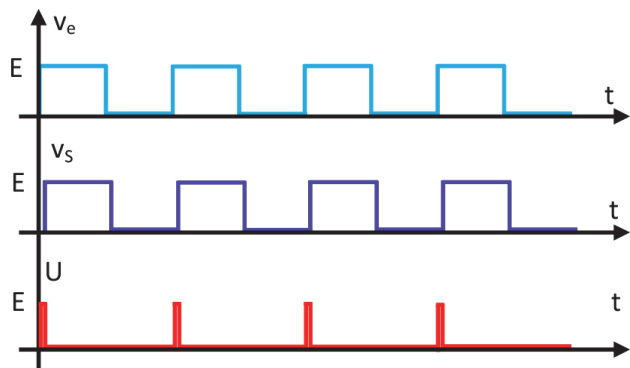


Figure 3.28a. Near-zero phase shift between v_e and v_s

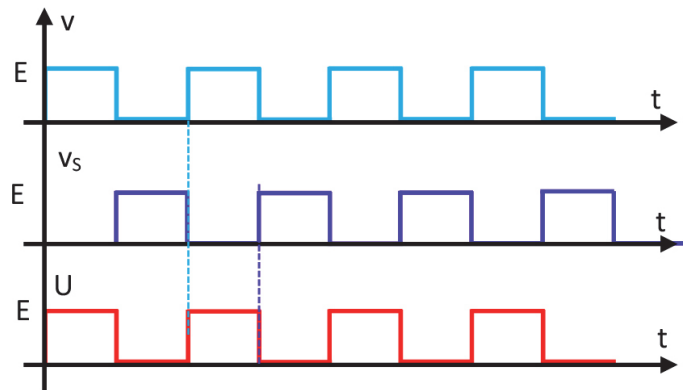


Figure 3.28b. Phase shift close to π between v_e and v_s

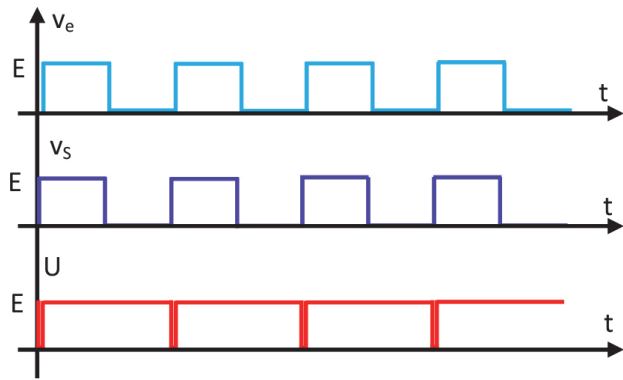


Figure 3.28c. Phase shift close to 2π between v_e and v_s

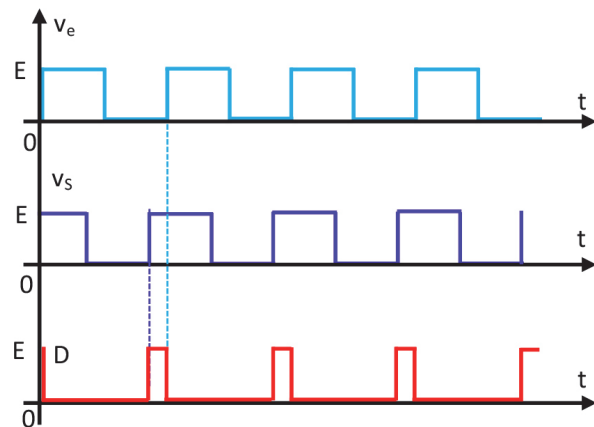


Figure 3.29. Signal $v_e(t)$ is lagging compared to signal $v_s(t)$. Signal D (Down) is active

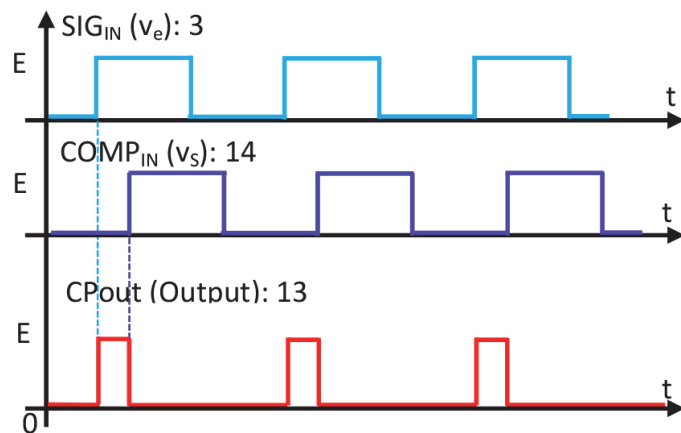


Figure 3.35. Input and output signals of the type-2 phase comparator of the 4046 IC (signal v_e is in leading phase compared to signal v_s)

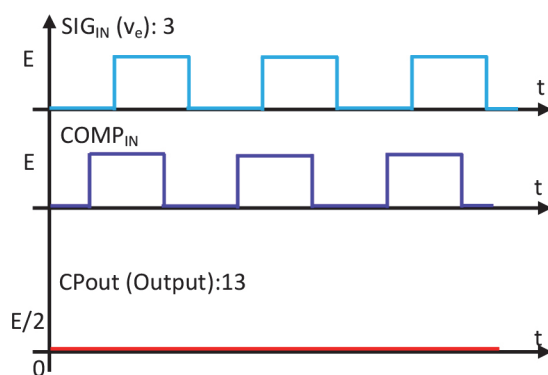


Figure 3.36. Input and output signals of the type-2 phase comparator of the 4046 IC (signal v_e is in lagging phase compared to signal v_s)

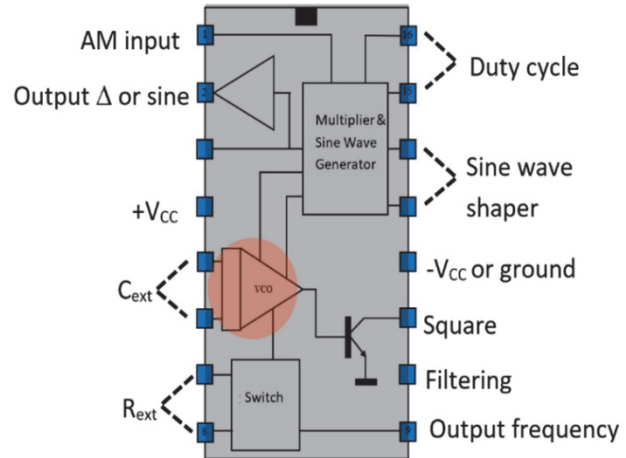


Figure 3.51. Internal diagram of the XR 2206 circuit

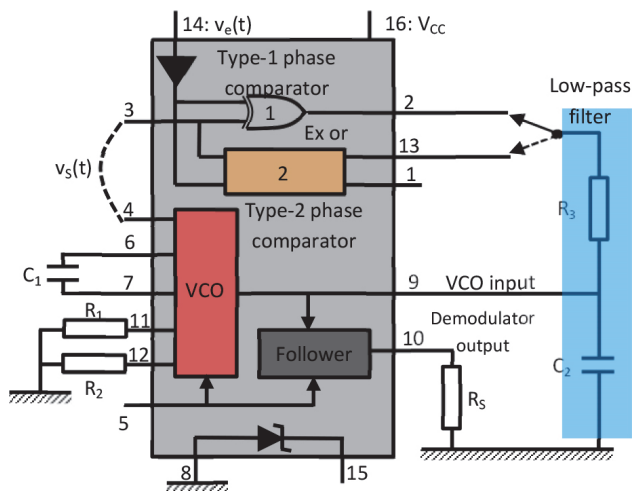


Figure 3.60. The 4046 IC and its block diagram

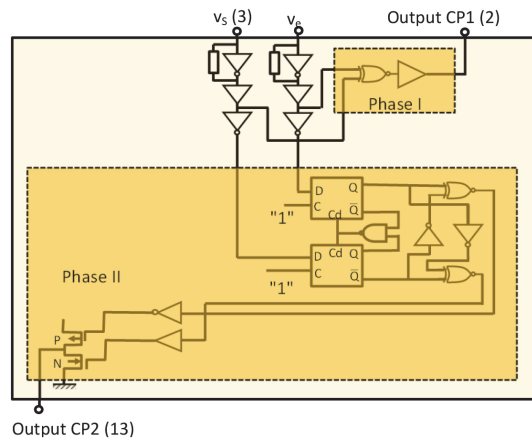


Figure 3.63. Schematic diagram of the two types of 4046 phase comparators

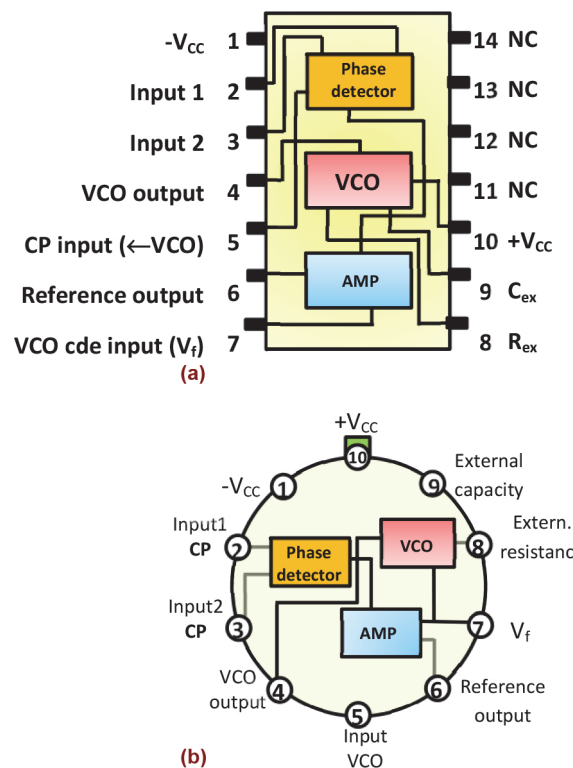


Figure 3.64. 565 PLL circuit in 14-pin DIL casing (a) and in 10-pin cylindrical-shape metal case (b)

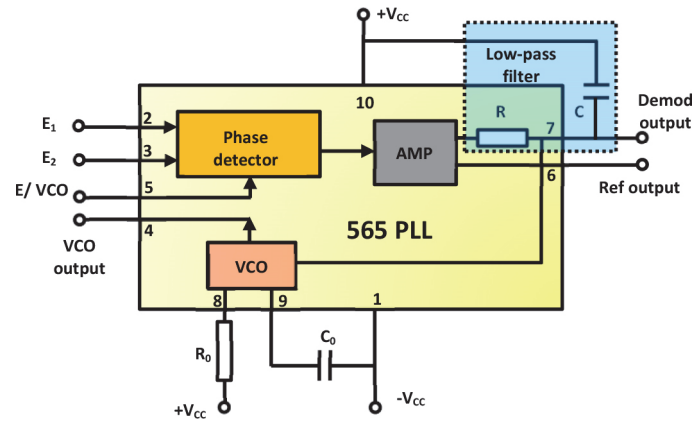


Figure 3.65. Block diagram of the 565 integrated PLL

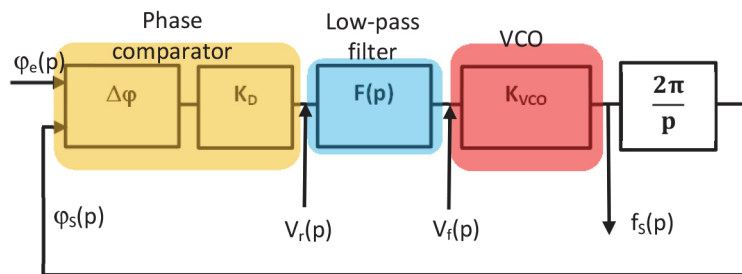


Figure 3.68. Block diagram of a PLL in terms of phase

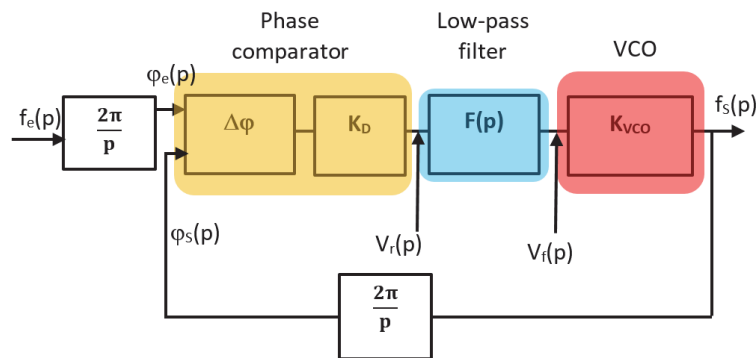


Figure 3.69. PLL block diagram; the input and output quantities are frequencies

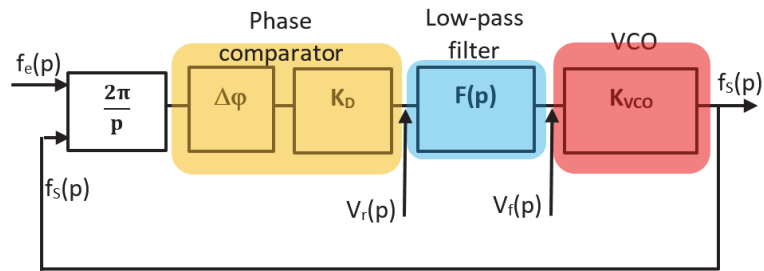


Figure 3.70. PLL block diagram in terms of frequency with unity feedback

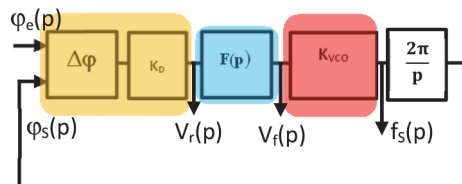


Figure 3.71. Diagram for the determination of the transfer function

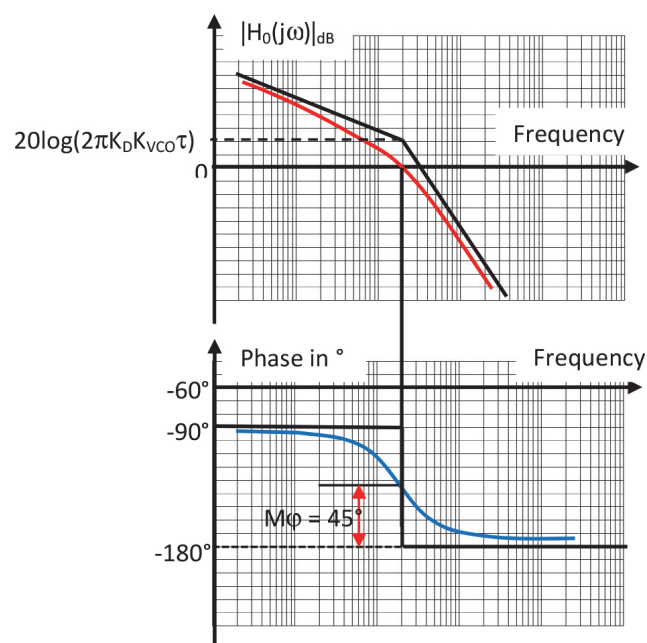


Figure 3.73. Bode plot of the open-loop transfer function of the PLL with a first-order low-pass RC-type loop filter

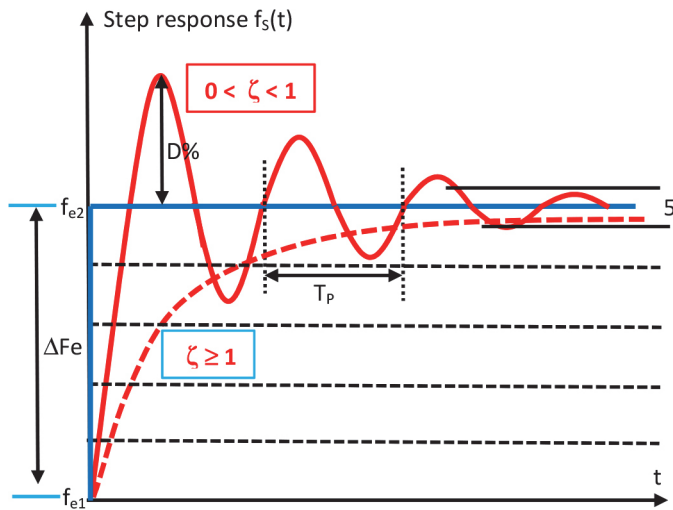


Figure 3.75. Second-order system step response

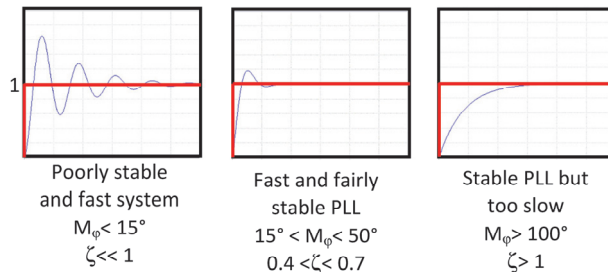


Figure 3.77. Evolution of a PLL step response according to the phase margin M_φ and the damping coefficient

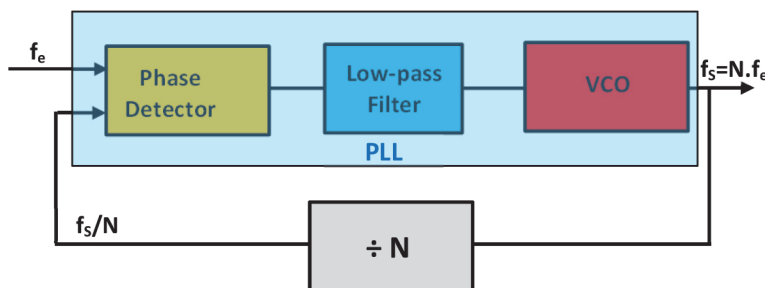


Figure 3.78. Principle of PLL-based frequency multiplying

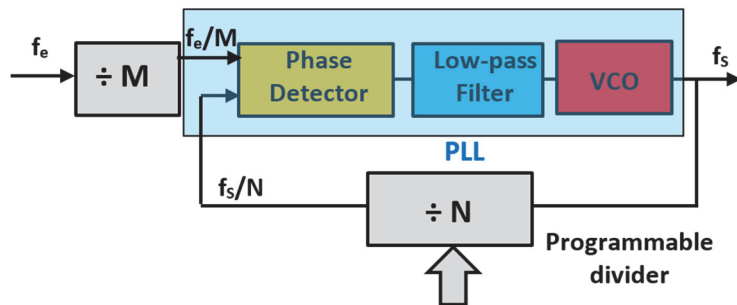


Figure 3.80. Principle of frequency synthesis using a PLL

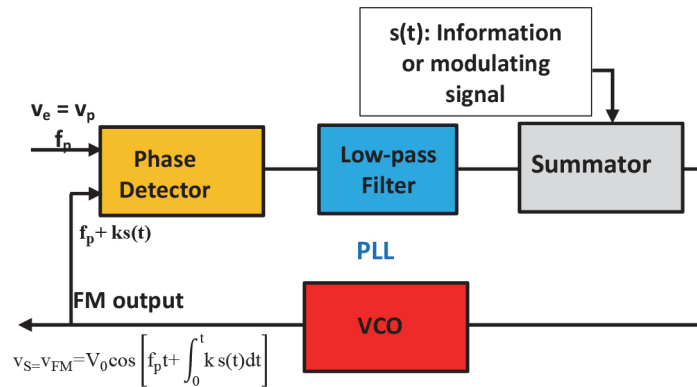


Figure 3.81. Frequency modulation using a PLL circuit

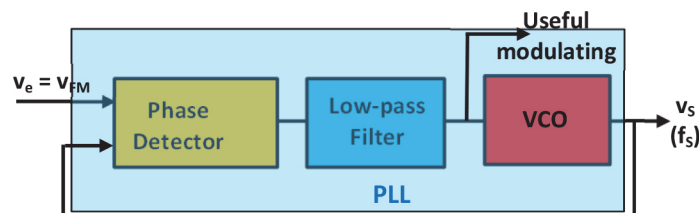


Figure 3.82. Frequency demodulation principle

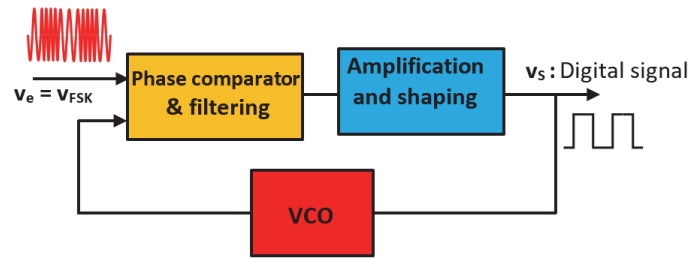


Figure 3.84. FSK demodulation principle

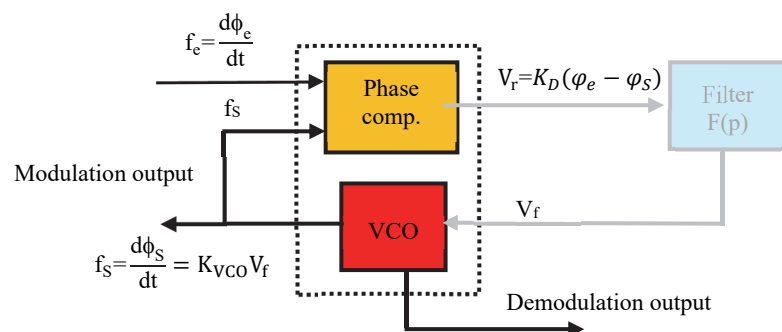


Figure 3.85. 4046 IC-based FSK modulation and demodulation

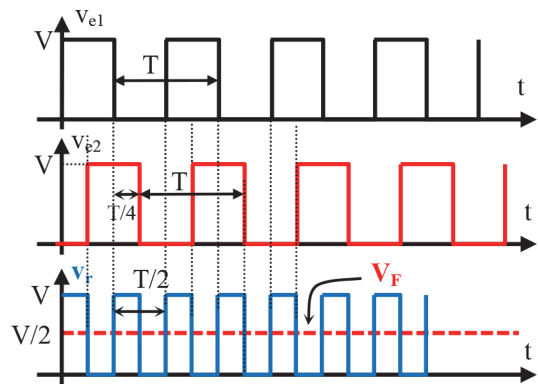


Figure E3.2. Representation of signals v_{e1} , v_{e2} , v_r and V_F

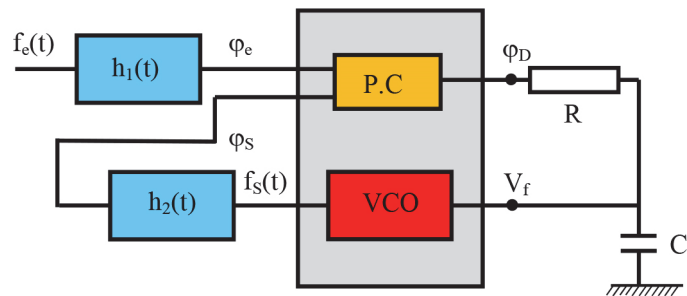


Figure E8.3. Block diagram under study

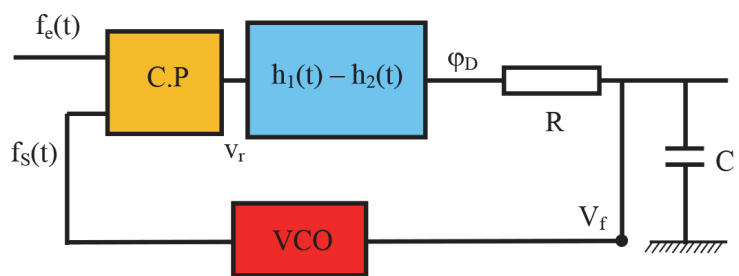


Figure E8.4. Simplified diagram of the PLL

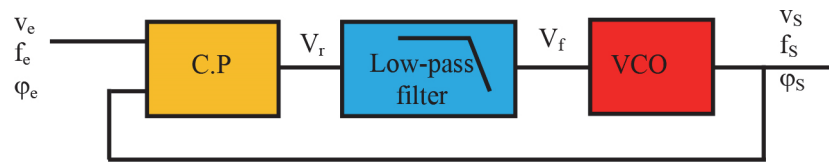


Figure E9.1. PLL circuit

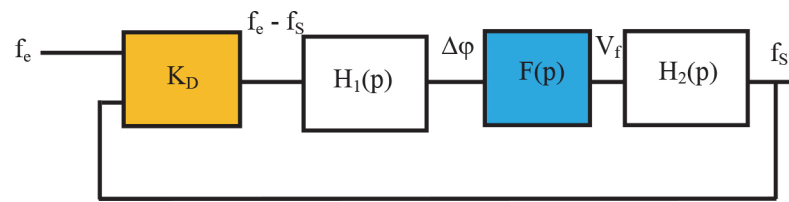


Figure E9.2. PLL block diagram

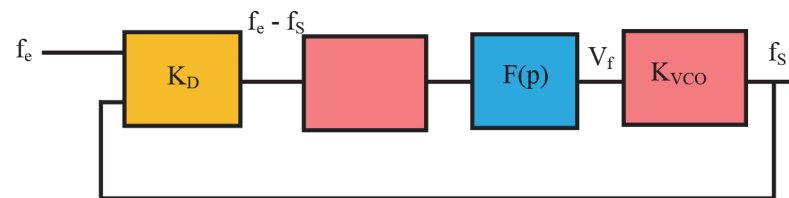


Figure E9.5. PLL block diagram with the definition of each block

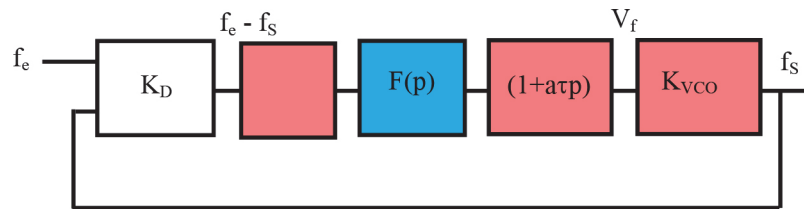


Figure E9.7. PLL block diagram with the low-pass filter of Figure E9.4

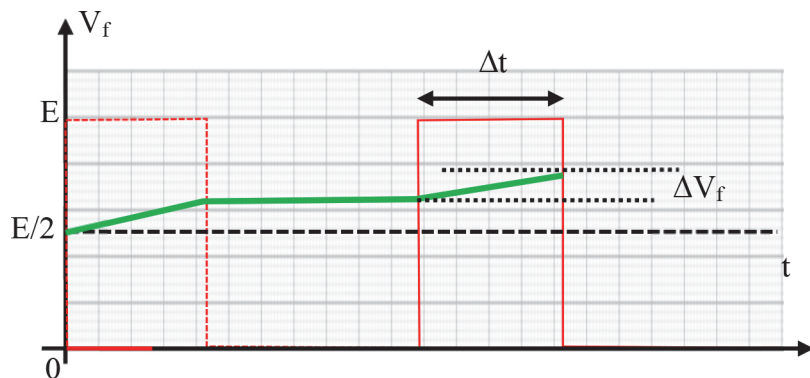


Figure E10.3. Evolution of voltage V_f at the capacitor terminals